JOM 23538

Heterocycles as ligands

XIX *. The electronic structure of 1,1'-diazametallocenes and the synthesis and crystal structure of 2,2',5,5'-tetra-tert-butyl-1,1'-diazanickelocene

Norbert Kuhn, Gerald Henkel, Jörg Kreutzberg and Stefan Stubenrauch

Fachbereich 6 (Chemie) der Universität (GH) Duisburg, Lotharstraße 1, D-47048 Duisburg (Germany)

Christoph Janiak

Institut für Anorganische und Analytische Chemie, Technische Universität Berlin, Straße des 17. Juni 135, D-10623 Berlin, Germany

(Received November 13, 1992)

Abstract

The electronic structure of diazaferrocene is shown to be similar to that of ferrocene and no evidence has been found for a conformational preference in the former. A smaller observed barrier for the ring rotation in the tetra-tert-butyl substituted diazaferrocene compared to that in the substituted ferrocene analog is attributed to more facile distortional modes in the heterocyclic system. Tetra-tert-butyl-diazanickelocene has been synthesized from $NiCl_2$ and $Li(C_4H_2{}^tBu_2N)$ and its crystal structure determined. Small, albeit significant structural differences in the diazaferrocene, -cobaltocene, -nickelocene series are explained in terms of the sequential filling of π-antibonding levels. In the bent Main Group species diazastannocene or -plumbocene an electronic situation different from that for the normal metallocenes gives rise to a conformational preference with both nitrogens pointing along the direction of maximum opening of the aza-Cp ring planes.

1. Introduction

Derivatives of 1,1'-diazaferrocenes (**1**) [2] were for some time regarded as incapable of existence following the unsuccessful work of Seel and Sperber on the parent compound [3]. However, stabilization of this structural type was eventually achieved through blocking of the nonbonding electron pairs on the nitrogen atoms, *e.g.* as in **2** [4] or through steric overcrowding of the α-positions (**3**) [5,6*]. This has stimulated discussion of the marked difference in stability of diazaferrocenes compared with that of the stable diphosphaferrocenes (**4**) [7] as well as of azaferrocene [8]. The instability of diazaferrocene was thought to arise possibly from repulsive interaction of the partially negatively charged nitrogen atoms [3] as well as from their basicity [9].
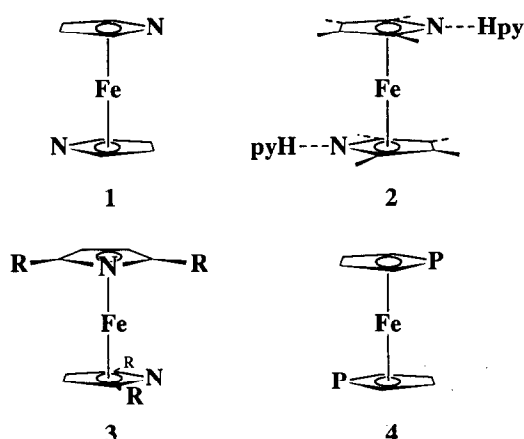
* Reference number with asterisk indicates a note in the list of references.

To provide a deeper understanding of this problem we have carried out molecular orbital calculations of the extended Hückel type on $M(C_4H_4N)_2$ (M = Fe, Co, Ni, Sn, and Pb) based on the structural data for the known compounds $M(2,5-C_4H_2{}^tBu_2N)_2$ with M = Fe [5], Co [10], Sn [11], Pb [12], as well as that with M = Ni, which is described here for the first time. We also tried to interpret the activation energies for the ligand movement in 2,2',5,5'-tetra-tert-butyl-1,1'-diazaferrocene (3, R = ^tBu) and the isoelectronic Co^{III} compound $[Co(2,5-C_4H_2{}^tBu_2N)_2]^+$ [10] compared with that for the structurally closely related 1,1',3,3'-tetra-tert-butylferrocene [13] which we recently investigated by temperature variable NMR spectroscopy [14].

2. Diazaferrocene

The electronic structure of diazaferrocene (1) is first briefly described by comparison with that of the analogous carbocyclic ferrocene. We begin with a comparison of the π-orbitals of $C_5H_5{}^-$ (5) [15] and $C_4H_4N^-$ (6).


5   **6**
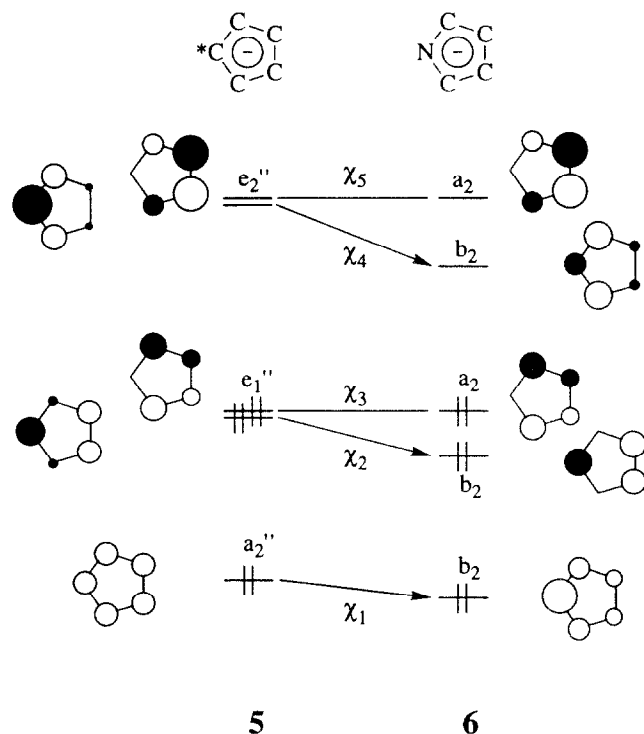
The perturbation encountered when the carbon atoms in a cyclic polyene are replaced by heteroatoms has been discussed in detail in several papers [16–18]. Replacing a C–H group by an isoelectronic, albeit more electronegative, nitrogen atom results in an electronic perturbation that removes the degeneracy of the e-levels (symmetry lowering from D_{5h} to C_{2v}). The orbitals with a coefficient on the replaced C-atom will

decrease in energy, while the others remain unaffected. Thus, χ_1, χ_2 and χ_4 are the orbitals lowered in energy. The resulting order of energies of the aza-Cp orbitals is depicted in 6 in comparison with that for 5.

The MO-diagram for diazaferrocene (not shown) is qualitatively very similar to that for ferrocene [17,19]. Consequently, the metal-based frontier orbitals of $Fe(C_4H_4N)_2$ are little affected when compared to those of $Fe(C_5H_5)_2$. As for unsubstituted ferrocene, the ring rotational barrier [20] for unsubstituted diazaferrocene can thus be expected to be very small, i.e. there should be no distinct conformational preference: the variation in the overlap population between the Fe and $(C_4H_4N)_2$ fragments with change in the rotational angle is too small to be regarded as significant. The maximum extended Hückel energy difference of 3.3 kJ mol^{-1} (1.5 kJ mol^{-1} for $Fe(C_5H_5)_2$) is too small to represent an important rotational barrier. Furthermore, a little more than half of this energy difference can be attributed to an inter-ring interaction, as can be seen by removing the iron center from the diazaferrocene complex and allowing the rings to rotate alone.

Another possible way of finding the conformational preferences in π complexes with heterocyclic systems, suggested by Hoffmann et al. [18,21], involves matching the donor and acceptor functions on the metal fragment with regions of high and low electron density in the heterocycle. This simple approach proved to be very informative in cases in which a polyene possessing a threefold localization of π donor orbitals interacts with three localized acceptor orbitals on a d^6-ML_3 fragment. Matching the π charge distribution of the pyrrolide anion (7) (corrected relative to a C_5H_5 anion, with a π charge of zero on each carbon [18]) to a d^6-MCp or M-aza-Cp fragment, however, fails to give a single interaction (overlap) of orbitals that influences the structure decisively due to the delocalization of the aza-Cp–metal bonds.

7
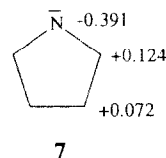
In summary, we cannot apply the criterion of minimum energy of certain 'key' orbitals (usually the HOMO, or an occupied MO close to it) in the conformational analysis (Walsh's rule) [22]. The Walsh diagram (orbital energies versus rotational angle) in Fig. 1 is inconclusive, as expected. There are no important level changes upon rotation of the N-atoms from a "syn" or 0° to an "anti" or 180° conformation. We just point out that the HOMO–LUMO gap in diazafer-
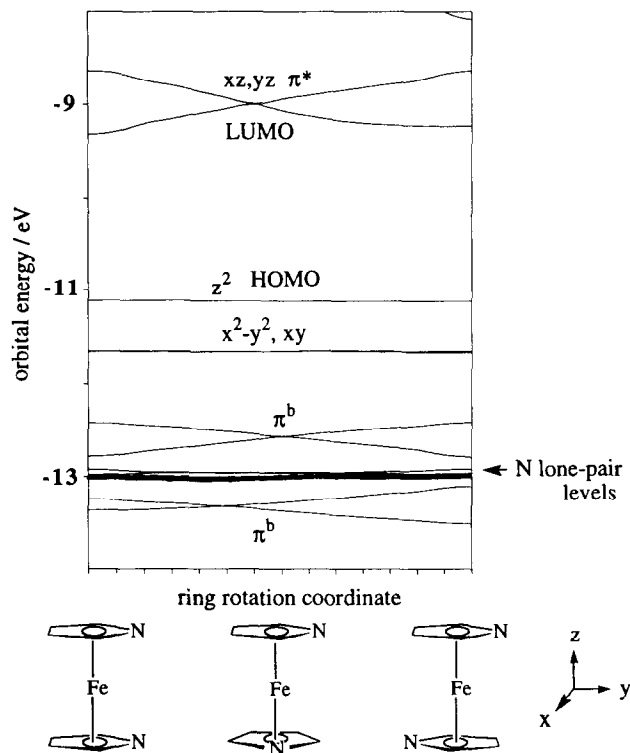
Fig. 1. Partial Walsh diagram, orbital energy *versus* rotational angle, for the rotation of one ring in diazaferrocene. The unchanged, resp. balanced changes in, orbital energies upon ring rotation do not lead to deviations in the total energy (bold curve, scaled to the energy of the orbital levels), and are thus indicative of a very low rotational barrier for the unsubstituted metallocene. The notation xy, $x^2 - y^2$ *etc.* stands for d_{xy}, $d_{x^2-y^2}$ orbitals *etc.*

rocene is smaller (by 0.5 to 0.8 eV, depending on the angle) than that for ferrocene or diphosphaferrocene within the extended Hückel framework. This indicates a lower stability and higher reactivity [23] for the dipyrrolide sandwich compound relative to those for the dicyclopentadienyl or diphosphacyclopentadienyl analog.

We note that a rather weak conformational preference was also deduced by Kostic and Fenske for the diphosphaferrocene analog [24]. Our analysis of the electronic structure and a possible preferential conformation in diazaferrocene is closely related to that by Gimarc and Starr [25] on the $(H_4B_2N_3)_2Fe$ complex [26] containing the inorganic aromatic $H_4B_2N_3$ rings (8). Compound 8 can be converted into the pyrrolide anion by the isoelectronic substitution of C–C by B–N groups.

8
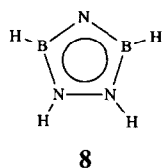
With respect to the conformational angle of 88° observed in the structure of bis(2,5-di-tert-butylpyrrol-lyl)iron (3, R = ¹Bu) [5], we conclude that the Fe–(aza-Cp) interaction contributes little to this preferential geometry. Instead the conformational preference must be ascribed to the steric interaction between the bulky tert-butyl groups, which seek to assume a staggered geometry (see below). And it is this staggered conformation that at the same time determines the N–N rotational angle. The very same structural feature has been observed in the carbocyclic bis(1,3-di-tert-butyl-cyclopentadienyl)iron [13]; in that case, the unique carbons (between the tert-butyl groups) were also found to be rotated by an angle of close to 90°, just like the nitrogens in 3.

## 3. Ligand movement in (substituted) ferrocene and diazaferrocene

In the light of the very similar electronic structures of ferrocene and diazaferrocene one would not expect substantially different barriers to ring rotation. Thus, the significantly smaller experimental barrier for the proton exchange in tetra-tert-butyldiazaferrocene (41.4 kJ mol⁻¹) compared to that in tetra-tert-butylferrocene (55.2 kJ mol⁻¹) was at first surprising [14]. The overall large experimental barriers compared to those for the unsubstituted metallocenes are, of course, due to steric hindrance between the bulky tert-butyl groups.

We can rationalize the experimentally found order for the tetra-tert-butyl substituted complexes in terms of two effects, *viz*: (1) The (aza-Cp)–Fe–(aza-Cp) geometry is more prone to distortion than Cp–Fe–Cp, and (2) the substituted aza-Cp is more amenable to an intraligand distortion than a normal Cp ligand.

3.1. Distortion in the ligand–Fe–ligand geometry

Since there is a somewhat weaker ring–metal bond (as indicated by the overlap population), it can be assumed that the aza-Cp fragment is more easily displaceable from its energetic minimum position in the diaza-Cp complex than is the Cp fragment in ferrocene. We suggest below possible distortions in the aza-Cp–iron bond which could lead to a smaller "rotational" barrier:

(a) The changes in total energy (not shown) for the asymmetric stretch (9) indicate an easier mode of displacement for aza-Cp than for normal Cp, which would help to account for a smaller barrier of rotation.

9
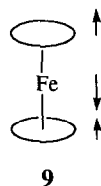
(b) For diazaferrocene the destabilization encountered upon ring slippage (as in **10** from the pentahapto position to a carbon atom, or in case of the aza-Cp to the nitrogen heteroatom) is much less than that for ferrocene. Part of this lower increase in energy for diazaferrocene is due to a decrease in the Fe–N distance and a greater Fe–N interaction which partly compensates for the loss in Fe–C overlap. Model studies indicate that a ring slippage will allow easier passage of the tert-butyl substituents upon rotation.
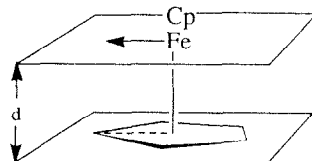
10

(c) An inward tilt of C-2,5 in the aza-Cp ring, as depicted in **11**, is also less destabilizing than the corresponding tilt in ferrocene. And a tilt along C-2 disentangles the bulky substituent on the 5-carbon from those on the opposite ring, thereby lowering the barrier of rotation.
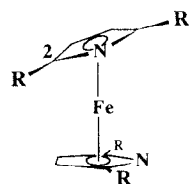
11

3.2. Intraligand distortion

A molecular modelling MNDO-calculation was carried out with two parallel 2,5-di-tert-butyl cyclopentadienyls, respectively, -azacyclopentadienyl rings and the metal being replaced by a + +-sparkle. The rings were rotated in opposite directions and the geometry was optimized in 10° steps with the rings fixed in a parallel disposition and the inter-ring distance as well as the C_5 or NC_4 ring geometry kept rigid. The internal parameters of the tert-butyl group and the *ipso*-C-ring parameters were, however, allowed to vary; in particular, the tert-butyl-group could bent out of the ring plane. Figure 2 shows the torsional diagram for the two di-tert-butyl-azacyclopentadienyl rings. The curves for two di-tert-butyl-cyclopentadienyl rings are very similar, except that the height of the rotational barrier between 90 and 180° is somewhat larger.

It is evident in Fig. 2 that there are two rather different rotational barriers, one at 0° and one at *ca.* 144°. The ring rotamers are sketched in Fig. 2 to help reveal the origin and nature of the maxima and min-
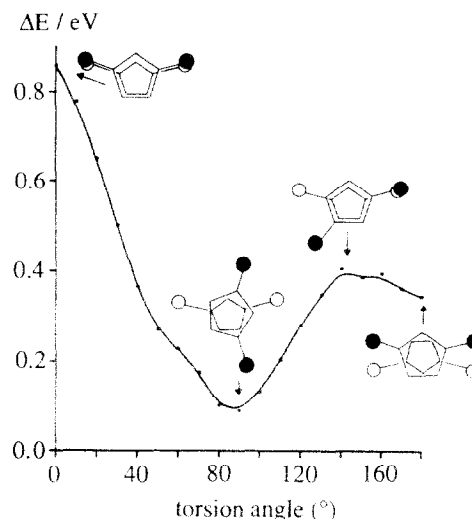

Fig. 2. Torsional diagram based on an MNDO-calculation for two parallel di-tert-butyl-azacyclopentadienyl rings with no metal in between. The curve for the carbocyclic di-tert-butyl-Cp analog is qualitatively very similar, only the barrier heights are different (see text). The sketches correspond to ring rotamers with torsional angles of 0, 90, 144, and 180°.
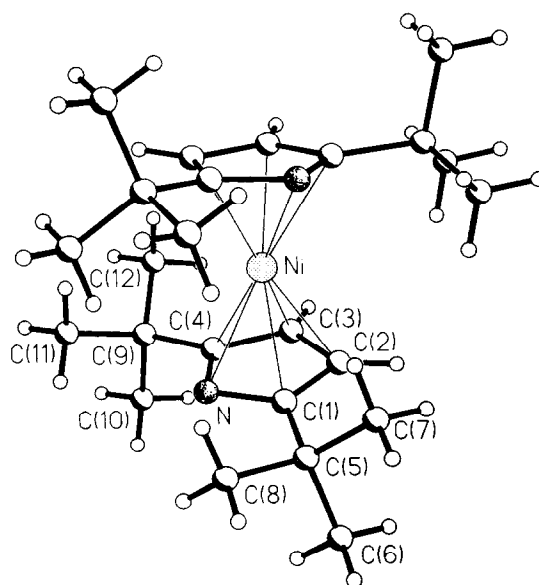
ima. The high barrier at 0° corresponds to a fully eclipsed conformation with respect to the tert-butyl groups (see sketches), whereas the smaller barrier at 144° represents a conformer with just two of the bulky substituents in the eclipsed position ("semi-eclipsed"). The well-defined minimum at ~ 90° is that for the fully staggered rotamer that is structurally observed [5,13]. The rather shallow minimum at 180° is for the semi-staggered conformation (see sketch). The large difference in barrier heights is easily rationalized on the basis of the conformer drawings given. It is very likely that a full ring rotation involving the fully eclipsed rotamer may not be feasible. Instead the ring motion may be essentially a back-and-forth movement between the fully-staggered minima at ±90° over the semi-eclipsed conformation. Such a back-and-forth movement results in an exchange between two enantiomeric forms which can be observed on the NMR time scale. The results of dynamic NMR studies have been analyzed on the basis of this restricted rotation

The MNDO calculation under the restrictions described above gives a rotational barrier of about 38.5 kJ mol^{-1} for two di-tert-butyl-Cp rings and 28.0 kJ mol^{-1} for the tetra-tert-butyl diaza-Cp analog. The order matches the experimental observation [14]. We can trace the smaller value for the di-tert-butyl-aza-Cp system to a higher flexibility in the *ipso*-C-ring bond, which allows the tert-butyl group to bend somewhat further out of the aza-Cp than out of the normal-Cp ring plane.

TABLE 1. Ni(C$_4$H$_2$^{t}Bu$_2$N)$_2$ (12): Coordinates and coefficients of the equivalent isotropic temperature factors (without H-atoms) [a]

| Atom	x	y	z	U [b]
Ni	0	0.5	0.1099(1)	0.018(1)
N	0.2366(8)	0.4458(7)	0.1356(2)	0.019(2)
C1	0.2064(8)	0.5994(8)	0.1410(3)	0.016(2)
C2	0.1772(9)	0.6689(11)	0.1006(2)	0.024(3)
C3	0.1926(8)	0.5513(8)	0.0698(2)	0.018(2)
C4	0.2295(9)	0.4159(9)	0.0919(2)	0.020(3)
C5	0.2253(9)	0.6788(8)	0.1835(2)	0.020(3)
C6	0.3790(9)	0.7669(10)	0.1837(2)	0.037(3)
C7	0.0960(9)	0.7921(8)	0.1910(2)	0.030(3)
C8	0.2277(9)	0.5627(8)	0.2205(2)	0.038(3)
C9	0.2703(9)	0.2610(9)	0.0736(2)	0.024(2)
C10	0.4421(8)	0.2641(8)	0.0627(2)	0.030(3)
C11	0.2426(9)	0.1330(8)	0.1060(2)	0.033(3)
C12	0.1795(9)	0.2260(9)	0.0331(2)	0.035(3)

[a] Estimated standard deviations of the last significant figure are given in parentheses. [b] The isotropic equivalent thermal parameter U is defined as one third of the trace of the orthogonalized U_{ij}-tensor.

4. Diazacobaltocene and -nickelocene

4.1. Synthesis and structure of 2,2',5,5'-tetra-tert-butyl-1,1'-diazanickelocene (12)

The synthesis of diazanickelocene (12) was carried out by a procedure analogous to that used for the iron [5] and cobalt [10] analog. Reaction of NiCl$_2$ with lithiated 2,5-di-tert-butylpyrrol gave 12 as a dark-green paramagnetic solid in good yield. The air-sensitive compound decomposes upon heating to elementary nickel and oligomeric coupling products of the pyrrolyl radical. Such coupling products were also observed from the reaction of 12 with neutral ligands such as pyridine or PR$_3$.
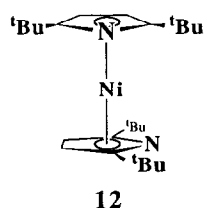
12

Atomic coordinates for 12 are listed in Table 1. Figure 3 shows a perspective drawing of a molecule along with the numbering scheme used. Bond distances and angles are summarized in Table 2. Complex 12 crystallizes in the space group $P\bar{4}2_1c$ isomorphous to the analogous iron [5] and cobalt [10] compounds. Despite the similarity of the ligand arrangement in the iron-cobalt-nickel series, the molecular geometry shows some significant differences, which are discussed below.

Fig. 3. Perspective drawing of one molecule of Ni(C$_4$H$_2$^{t}Bu$_2$N)$_2$, 12.

4.2. Electronic structure

The electronic structures of diazacobaltocene and -nickelocene can be qualitatively depicted by the same interaction diagram as for diazaferrocene and ferrocene, respectively [17,19], except that in the latter species there are one, or in the second case, two more electrons which enter the metal based π-antibonding levels. This occupation of metal-ligand antibonding orbitals results in weakening of the metal–ligand bond, and this in turn causes a lengthening of the metal–C/N distances (see Table 3). The same effect is observed for the carbocyclic ferrocene, cobaltocene, and nickelocene series [27].
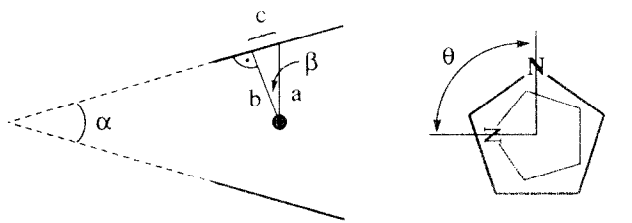
However, for the diaza compounds we find an additional difference in structure, as judged from the tetra-tert-butyl substituted species. Upon going from

TABLE 2. Bond distances (pm) and angles (°) [a] for Ni(C$_4$H$_2$^{t}Bu$_2$N)$_2$ (12)

Distances			
Ni–N	225.7(7) (2×)	C1–C2	141.7(10)
Ni–C1	221.4(7) (2×)	C2–C3	140.8(10)
Ni–C2	214.8(8) (2×)	C3–C4	140.1(10)
Ni–C3	213.6(7) (2×)	C4–N	138.5(10)
Ni–C4	219.8(8) (2×)	C1–C5	150.0(11)
N–C1	137.2(9)	C4–C9	150.5(11)

Angles			
N–C1–C2	110.0(7)	C4–N–C1	107.0(7)
C1–C2–C3	106.1(7)	N–C1–C5	122.3(7)
C2–C3–C4	107.3(6)	N–C4–C9	121.9(7)
C3–C4–N	109.6(6)		

[a] Additional relevant parameters for the Ni–ligand and inter-ligand geometry can be found in Table 3.

TABLE 3. Changes in the metal–ligand and ligand–ligand geometry for $M(C_4H_2^tBu_2N)_2$ (M = Fe, Co, Ni)

M	Fe	Co	Ni
M–C (av.) (pm)	205.9	211.6	217.3
M–N (pm)	208.7	217.6	225.8
α (°) [a]	7.7	8.8	10.4
β (°) [b]	0.0	1.9	3.8
θ (°) [c]	88.5	85.2	86.6
a (pm) [d]	168.3	175.8	184.1
b (pm) [e]	168.3	175.7	183.7
c (pm) [f]	0.0	5.9	12.1

[a] Angle made by the two ring planes at their intersection. [b] Angle made by the projections b and c, of the metal atom onto the ring plane. [c] Torsional angle defined by the connectivity N–(ring centroid)–(ring centroid)–N. [d] Line joining the ring centroid to the metal atom. [e] The projection of the metal atom onto the ring plane; the ring normal to the metal atom. [f] The distance between the ring centroid and the normal to the metal atom, calculated according to $c = (a^2 - b^2)^{1/2}$.

Fe [5] to Co [10] to Ni, the metal slips away from the position over the ring center, thereby increasing the M–N distance relative to M–C (Table 3). We can account for the metal movement away from the nitrogen atoms in terms of the contribution of the newly filled orbitals to the metal-ring atom overlap population. Filling the π-antibonding levels with one or two electrons decreases the overlap population between the central metal and all the ring atoms. The metal-nitrogen overlap is, however, especially reduced, resulting in an essentially nonbonding metal–nitrogen interaction if the π^*-levels were filled with two electrons. The variation of the overlap population as a function of electron occupation is illustrated in Fig. 4 for the case of diazaferrocene. The CACAO plots [28] in Fig. 4 illustrate the respective orbital characters and show the large coefficient of the wave function on the nitrogen atoms, out-of-phase or antibonding to the metal d-orbital.

5. Bent diazametallocenes

The question arises of whether we should find a conformational preference based on the metal–ring or ring–ring interactions if the pyrrolide rings were not parallel as in ferrocene but tilted towards each other.
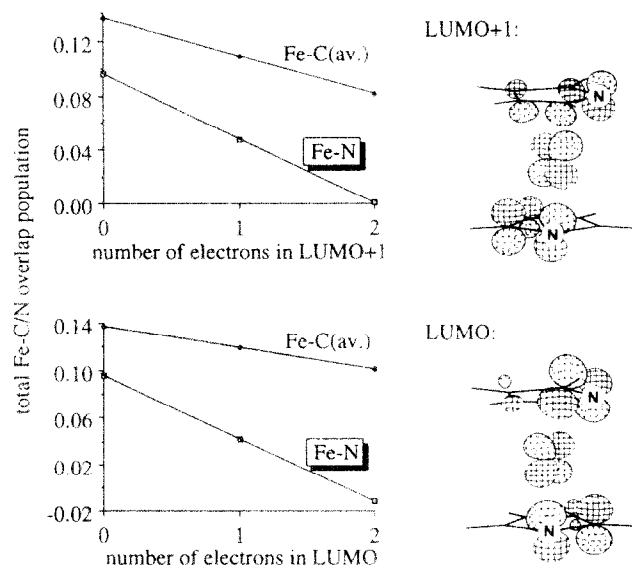

Fig. 4. The changes in the total Fe–ring atom overlap population in diazaferrocene when the two lowest unoccupied molecular orbitals are filled with one or two electrons. The sequential filling with electrons represents the transformation from diazaferrocene to diazacobaltocene to -nickelocene and explains the lengthening in metal–ring distances as well as the increase in deviation from an ideal metallocenic structure (cf. Table 3) as the metal–nitrogen interaction is weakened overproportionally compared with the metal–carbon interactions. The CACAO plots [28] at the right hand side illustrate the contributions of the atomic wavefunctions to the molecular orbital.

To check this, we studied diazametallocenes which have a bent structure, namely diazastannocene and diazaplumbocene (13).
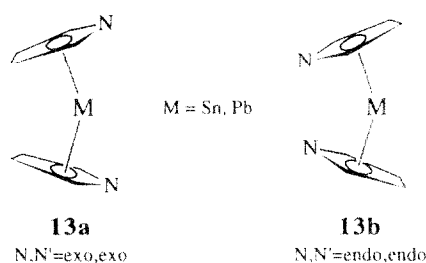
The 2,2',5,5'-tetra-tert-butyl substituted derivatives of 13 have been synthesized [11,12] and the crystal structure of the diazastannocene and -plumbocene derivative have been determined. In these solid-state structures the nitrogen atoms are oriented along the maximum opening of the Cp-ring planes. We refer to the nitrogen position in this conformation as exo (13a), and the orientation in which an N-atom points towards the intersecting line of the ring planes is termed endo (13b).

In light of the above results for diazaferrocene it was very surprising to find that rotating one or both nitrogens in unsubstituted diazastannocene from the

(experimental) *exo* into the *endo* position led to a large increase in the total energy (Fig. 5, bold curve). This increase in (extended Hückel) energy is about 1 eV if both rings are rotated from *exo* to *endo* which is quite a large effect.

Our initial assumption that the increase was due to a 2-orbital/4-electron repulsion of the nitrogen lone-pairs was easily disproved: setting the matrix elements for the overlap between the two nitrogen atoms to zero, gave the same increase in energy upon rotation. Instead, we can show with the help of the Walsh diagram in Fig. 5 that the increase in total energy closely parallels the increase in energy of the HOMO. The nitrogen lone-pair levels, in particular, do not change in energy on going from the *exo,exo* to the *endo,endo* conformation.

For stannocene and diazastannocene the highest occupied molecular orbital is calculated on the extended Hückel level to be essentially a tin lone-pair orbital [29]. In regard to the energetic order, these semiempirical MO calculations have been replaced by

Fig. 6. Reduced overlap population between Sn and C_5H_5 or C_4H_4N in stannocene, respectively diazastannocene as a function of the ring-rotational conformation. The upper two curves represent the total overlap population, while the lower ones give the contribution from the HOMO, derived from an orbital by orbital decomposition of the overlap population. Note the decrease in overlap population for diazastannocene towards the *endo,endo* conformer.
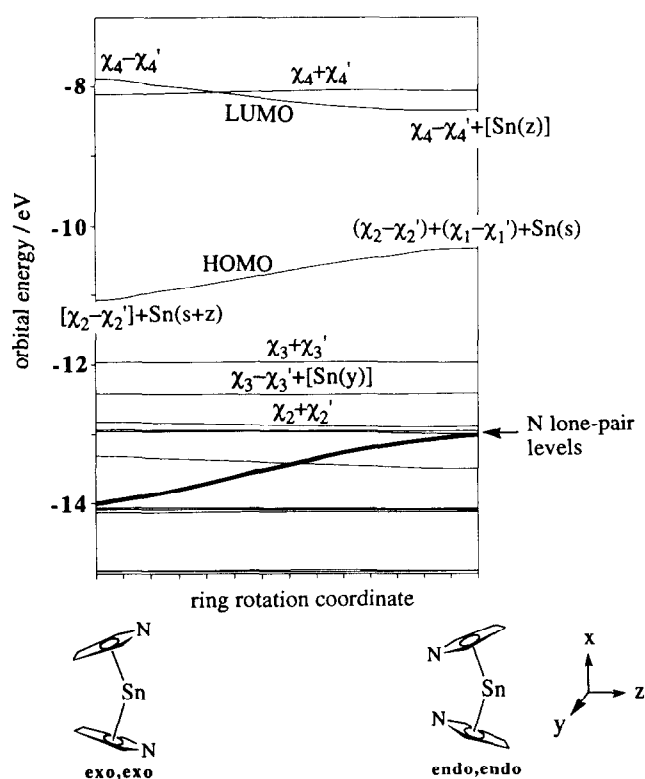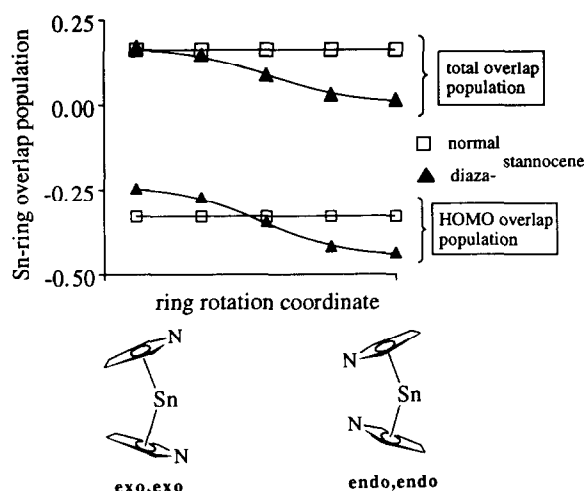

Fig. 5. Walsh diagram for the ring rotation from the *exo,exo* to the *endo,endo* conformation in diazastannocene. Minor orbital contributions are given in brackets. For a representation of χ_i see 6. Note the demixing of Sn(z) from the HOMO together with its energy increase, which parallels the change in total energy (bold curve, scaled to the energy of the orbital levels). The notation Sn(s), Sn(z) etc. stands for the s, p_z etc. orbitals on tin.

SCF-Xα-SW results [30], which put the lone-pair in a strongly directional, fifth-occupied orbital *ca.* 2 eV more stable than the HOMO. Here, however, it is not the relative energetic position but the substantially antibonding character of the HOMO that will prove important.

An orbital-by-orbital decomposition of the overlap population between the tin center and one ring gives values of -0.331 and -0.245 for the HOMO in stannocene and diazastannocene (*exo,exo*) compared to a total Sn–ring overlap population of 0.163 and 0.170. Much experience shows that a larger positive overlap population correlates with a stronger bond and a larger bond order between atoms A and B.

While the overlap population values for stannocene are invariant with respect to a ring rotation as expected, the overlap population of the HOMO in diazastannocene becomes much more negative in the *endo,endo* conformation (-0.437). Figure 6 illustrates this change that is responsible for the overall sharp drop in the total Sn–aza-Cp ring overlap population from 0.170 to 0.015. The overlap population of the bonding levels does not change much.

This decrease in overlap population is the origin of the increase in the energy of the HOMO and so of the total energy for diazastannocene. We can further correlate the variation in the HOMO overlap population with the magnitude of the Sn p contribution. The fall in overlap population on going from the *exo,exo* to the *endo,endo* conformation in diazastannocene is accompanied by a fall in the Sn p_z contribution to the

HOMO from 20 to 5%. The intermediate HOMO overlap population in normal stannocene has a constant p contribution of 14%. In diazastannocene the p_z orbital mixes from the HOMO into the LUMO as the LUMO is lowered in energy from *exo,exo* to *endo,endo* (see Fig. 5), and matches the p-orbital energy on the tin atom ($H_{5p} = -8.32$ eV).

The Walsh diagram in Fig. 5 reveals the decrease in the HOMO–LUMO gap upon ring rotation in diazastannocene, thereby indicating a lower stability and higher reactivity in the *endo,endo* conformation. Both the decrease in HOMO–LUMO gap and the drop in Sn–ring overlap population upon ring rotation may help to account for the nonexistence of an η^5-bonded unsubstituted diazastannocene. The bulky tert-butyl substituents in the 2,5-positions can thus be thought of as preventing not only an unstable η^1 N–Sn coordination mode but also an *endo,endo* conformation by blocking the ring rotation.

We have referred only to diazastannocene when discussing the electronic structure of a bent diazametallocene, but the heavier analog diazaplumbocene shows exactly the same electronic features in respect of comparison between the *exo,exo* to the *endo,endo* conformation.

6. Conclusion

A frontier molecular orbital analysis of unsubstituted ferrocene and diazaferrocene based on orbital energy and overlap has failed to show evidence for a conformational preference. The rotational barrier in the hypothetical unsubstituted diazaferrocene will be very low, as in ferrocene. The conformation encountered in the tetra-tert-butyl substituted diazaferrocene with an 88° rotation of the nitrogens must be attributed solely to the bulky tert-butyl groups and their attempt to assume a staggered geometry.

The smaller experimental barrier for the proton exchange in 2,2',5,5'-tetra-tert-butyl diazaferrocene compared with that for the 1,1',3,3'-tetrasubstituted ferrocene analog cannot be accounted for in terms of a smaller barrier for a simple Cp (resp. aza-Cp)–Fe rotation. We have shown, however, that both the (aza-Cp)–Fe–(aza-Cp) geometry as well as the tert-butyl substituted aza-Cp ligand alone, are more prone to certain kinds of distortions (which can facilitate the passage of the bulky ring substituents) than the carbocyclic systems.

The structures of tetra-tert-butyl-diazaferrocene and -cobaltocene and the novel -nickelocene analog have been compared, and small, but significant deviations explained in terms of sequential filling of metal–ring π-antibonding levels, accompanied by a stronger de-crease in metal–nitrogen than metal–carbon overlap population.

In the cases of bent Main Group diazametallocenes (*e.g.* diazastannocene or -plumbocene) the electronic situation in the metal–ring interaction changes in such a way that a strong conformational preference arises. A conformation with both ring nitrogens pointing along the maximum opening of the aza-Cp ring-planes (*exo,exo* form) is strongly preferred on the basis of Sn–ring overlap and orbital energy criteria.

7. Theoretical section

The computations were performed within the extended Hückel formalism [31] with weighted H_{ij}'s [32]. The program (ICON) was kindly supplied by R. Hoffmann (Cornell University, Ithaca, NY). The atomic parameters for the elements involved in our calculations are given in Table 4. The iron parameters were derived by a charge iteration on the ferrocene molecule. Geometrical parameters were fixed as follows: Fe–C/N = 206.5, Sn–C/N = 271.4, Pb–C/N = 275.0, C–C/N = 142, C–H = 96 pm; Cp–Sn–Cp and Cp–Pb–Cp = 140° (Cp denotes the ring center), C–C–C, C–C–N, and C–N–C = 108°, unless otherwise indicated.

8. Experimental section

8.1. Synthesis of 2,2',5,5'-tetra-tert-butyl-1,1'-diazanickelocene (12)

Tetrahydrofuran (20 ml) was added to a mixture of 0.98 g (7.5 mmol) of $NiCl_2$ and 2.80 g (15.0 mmol) of lithiated di-tert-butylpyrrole (formed quantitatively from di-tert-butylpyrrole and n-butyllithium in hexane

TABLE 4. Parameters used in the extended Hückel calculations

Atom	Orbital	H_{ii}(eV)[a]	ζ_1[b] (c_1[c])	ζ_2[b] (c_2[c])	Ref.
Fe	4s	−9.43	1.90		[d]
	4p	−5.24	1.90		
	3d	−11.50	5.35 (0.5505)	2.00 (0.6260)	
Sn	5s	−16.16	2.12		33
	5p	−8.32	1.82		
Pb	6s	−15.7	2.35		34
	6p	−8.0	2.06		
N	2s	−26.0	1.95		31
	2p	−13.4	1.95		
C	2s	−21.4	1.625		31
	2p	−11.4	1.625		
H	1s	−13.6	1.3		31

[a] Orbital energies. [b] Slater exponents. [c] Coefficients used in the double ζ expansion of the d orbitals. [d] Parameters obtained by a charge iteration on ferrocene.

[5]). The mixture was refluxed for 30 min and the volatile components were then removed *in vacuo*. The residue was extracted with 60 ml n-pentane, and 2.42 g (78%) of dark-green crystals of **12** obtained upon cooling of the extract. M.p. 78°C, dec. MS (70 eV): m/e = 414 (13%, M^+), 399 (3, $[M - Me]^+$), 179 (66%, $[C_4H_2{}^tBu_2NH]^+$), 164 (100, $[C_4H_2{}^tBu_2NH^+ - Me]$) and further fragments. Analysis. Found: C, 69.17; H, 9.26; Ni, 14.70. $C_{24}H_{40}N_2Ni$ (415.37); calc.: C, 69.39; H, 9.73; Ni, 14.13%.

8.2. X-ray structure determination

A single crystal of $Ni(C_4H_2{}^tBu_2N)_2$ suitable for X-ray diffraction was fixed on the top of a glass fiber which was mounted in the center of a Siemens P4RA four-circle diffractometer. The specimen was cooled down to *ca*. 150 K under a stream of cold nitrogen gas by using a modified SYNTEX LT-2 cooling device. The orientation matrix and the unit cell dimensions were obtained by a least-squares fit of the setting angles of 18 centred reflections in the range $20° < 2\theta < 30°$. The intensities of two standard reflections monitored every 98 scans showed no significant changes during data collection. The intensity profiles of all reflections indicated stable crystal settings during the

measurements. All calculations including data reduction (Lorentz and polarisation corrections) and empirical absorption corrections were carried out by use of the SHELXTL PLUS program package [35] on an MS-DOS personal computer with an Intel 80486 microprocessor. The structure was solved by direct methods and refined with hydrogen atoms fixed at idealized positions (C–H = 96 pm). Atomic scattering factors for spherical neutral free atoms (bonded for hydrogen) were taken from standard sources [36]. Both the f' and f'' components of the anomalous dispersion [36] were included for all non-hydrogen atoms. They were refined anisotropically during the last stage of the refinement. Further details of the data collection and structure refinement including final R values are shown in Table 5 [37*].

Acknowledgements

TABLE 5. Crystallographic data for $Ni(C_4H_2{}^tBu_2N)_2$ (**12**)

Empirical formula	$C_{24}H_{40}N_2Ni$
F.W.	415.29
Crystal size, mm	ca. $0.18 \cdot 0.14 \cdot 0.12$
Temperature, K	150
Crystal system	tetragonal
Space group	$P\bar{4}2_1c$
a, pm	869.5(1)
c, pm	3108.6(6)
V, pm³	$2350 \cdot 10^6$
Z	4
$\mu(Mo\ K\alpha)$, mm^{-1}	0.84
D_{calc}, g cm^{-3}	1.174
Measuring device	Siemens P4 four-circle diffractometer, (rotating anode generator, graphite monochromator, scintillation counter, λ = 71.073 pm (Mo Kα))
Scan type	ω-scan
Absorption correction	empirical (ψ-scan)
Transmission range	0.767–0.723
Scan range	$4° < 2\theta < 48°$ ($+h$, $+k$, $+l$)
Scan speed	intensity dependent (3 to 29° min^{-1})
Structure solution	SHELXTL PLUS (direct methods)
Structure refinement	full-matrix, least squares, non-hydrogen atoms anisotropic, hydrogen atoms at idealized positions (U_H = 1.2 · U_C), one scale factor, one isotropic extinction parameter
Weighting scheme	$w = [\sigma^2(F_o) + (0.01 \cdot F_o)^2]^{-1}$
Total number of reflections	2828
Number of independent reflections	1482, of which 845 are observed ($I > 2\sigma(I)$)
Number of variables	123
$R = (\Sigma \| F_o \| - \| F_c \|)/\Sigma \| F_o \|$	0.0488
$R_W = [\Sigma w(\| F_o \| - \| F_c \|)^2/\Sigma w F_o^2]^{1/2}$	0.0376

References and notes

1 Part XVIII: N. Kuhn, J. Kreutzberg, E.-M. Lampe, D. Bläser and R. Boese, J. Organomet. Chem., (JOM 23670) in press.
2 For a review, see: N. Kuhn, Bull. Soc. Chim. Belg., 99 (1990) 707.
3 F. Seel and V. Sperber, J. Organomet. Chem., 14 (1968) 405.
4 N. Kuhn, E.-M. Horn, R. Boese and N. Augart, Angew. Chem., 100 (1988) 1433; Angew. Chem., Int. Ed. Engl., 27 (1988) 579.
5 N. Kuhn, K. Jendral, R. Boese and D. Bläser, Chem. Ber., 124 (1991) 89.
6 Compare with the synthesis of bis(η^5-pyridin)chromium, which was only successful after blocking the α-positions by trimethylsilyl groups: C. Elschenbroich, J. Koch, J. Kroker, M. Wünsch, W. Massa, G. Baum and G. Stork, Chem. Ber., 121 (1988) 1983.
7 Review: F. Mathey, New J. Chem., 11 (1987) 585.
8 K.K. Joshi, P.L. Pauson, A.R. Quazi and W.H. Stubbs, J. Organomet. Chem., 1 (1964) 471; R.B. King and M.B. Bisnette, Inorg. Chem., 3 (1964) 796; for the stabilization of azaferrocene through methyl substituents, see: N. Kuhn, M. Schulten, E. Zauder, N. Augart and R. Boese, Chem. Ber., 122 (1989) 1891.
9 A. Efraty, N. Jubran and A. Goldman, Inorg. Chem., 21 (1982) 868.
10 N. Kuhn, M. Köckerling, S. Stubenrauch, D. Bläser and R. Boese, J. Chem. Soc., Chem. Commun., (1991) 1368.
11 N. Kuhn, G. Henkel and S. Stubenrauch, J. Chem. Soc., Chem. Commun., (1992) 760.
12 N. Kuhn, G. Henkel and S. Stubenrauch, Angew. Chem., 104 (1992) 766; Angew. Chem., Int. Ed. Engl., 31 (1992) 778.
13 T. Leigh, J. Chem. Soc., (1964) 3294; Z.L. Kaluski, A.I. Gusev, A.E. Kalinin and Y.T. Struchkov, Zh. Strukt. Khim., 13 (1972) 950; R. Boese, D. Bläser, N. Kuhn and S. Stubenrauch, Z. Kristallogr., 205 (1993) 282.
14 N. Kuhn, K. Jendral, S. Stubenrauch and R. Mynott, Inorg. Chim. Acta, 206 (1993) 1.
15 W.J. Jorgensen and L. Salem, The Organic Chemist's Book of Orbitals, Academic Press, New York, 1973, pp. 237–239; F.A. Cotton, Chemical Applications of Group Theory, 2nd edition, Wiley-Interscience, New York, 1971, p. 142.
16 E. Heilbronner and H. Bock, Das HMO-Modell und seine Anwendung, Verlag Chemie, Weinheim, 1986, pp. 132–167.
17 T.A. Albright, J.K. Burdett and M.H. Whangbo, Orbital Interactions in Chemistry, Wiley-Interscience, New York, 1985, p. 219ff.
18 T.A. Albright and R. Hoffmann, Chem. Ber., 111 (1978) 1578.
19 W. Moffitt, J. Am. Chem. Soc., 76 (1954) 3386; N.N. Greenwood and A. Earnshaw, Chemistry of the Elements, Pergamon Press, Oxford, 1984, p. 369ff; F.A. Cotton and G. Wilkinson, Advanced Inorganic Chemistry, 5th edition, Wiley, New York, 1988, pp. 80–81; C. Elschenbroich and A. Salzer, Organometallics, VCH Verlag, Weinheim, 1989, p. 318ff.

20 A. Haaland, Top. Curr. Chem., 53 (1975) 1, and refs. therein; A. Haaland and J.E. Nilsson, Acta Chem. Scan., 22 (1968) 2653; F. Rocquet, L. Berreby and J.P. Marsault, Spectrochim. Acta A, 29 (1973) 1101; L.N. Mulay and A. Attalla, J. Am. Chem. Soc., 85 (1963) 702; M.K. Makova, E.V. Leonova, Yu.S. Kaninov and N.S. Kochetkova, J. Organomet. Chem., 55 (1973) 185; A.J. Campbell, C.A. Fyfe, D. Harold-Smith and K.R. Jeffrey, Mol. Cryst. Liq. Cryst., 36 (1976) 1.
21 T.A. Albright, P. Hofmann and R. Hoffmann, J. Am. Chem. Soc., 99 (1977) 7546.
22 A.D. Walsh, J. Chem. Soc., (1953) 2260, 2266, 2288, 2296, 2301, 2306, 2318, 2321, 2325, 2330; L.C. Allen, Theor. Chim. Acta, 24 (1972) 117; R.J. Buenker and S.D. Peyerimhoff, Chem. Rev., 74 (1974) 127.
23 Z. Zhou and R.G. Parr, J. Am. Chem. Soc., 112 (1990) 5720, and refs. therein.
24 N.M. Kostic and R.F. Fenske, Organometallics, 2 (1983) 1008.
25 B.M. Gimarc and L.E. Starr, The Chemistry of Inorganic Ring Systems, in R. Stendel (Ed.), Studies in Inorganic Chemistry, Vol. 14, Elsevier, Amsterdam, 1992, p. 429 ff.
26 H. Nöth and W. Regnet, Z. Anorg. Allg. Chem., 352 (1967) 1.
27 W. Bünder and E. Weiss, J. Organomet. Chem., 92 (1975) 65; P. Seiler and J.D. Dunitz, Acta Crystallogr., Sect. B, 35 (1979) 1068 and 2020; P. Seiler and D. Dunitz, Acta Crystallogr., Sect. B, 36 (1980) 2255; A. Haaland, Acc. Chem. Res., 12 (1979) 415.
28 C. Mealli and D.M. Proserpio, J. Chem. Ed., 67 (1990) 399.
29 P. Jutzi, F. Kohl, P. Hofmann, C. Krüger and Y.H. Tsay, Chem. Ber., 113 (1980) 757.
30 S.G. Baxter, A.H. Cowley, J.G. Lasch, M. Lattman, W.P. Sharum and C.A. Stewart, J. Am. Chem. Soc., 104 (1982) 4064.
31 R. Hoffmann, J. Chem. Phys., 39 (1963) 1397; R. Hoffmann and W.N. Lipscomb, J. Chem. Phys., 36 (1962) 2179; R. Hoffmann and W.N. Lipscomb, J. Chem. Phys., 37 (1962) 2872.
32 J.H. Ammeter, H.-B. Bürgi, J.C. Thibeault and R. Hoffmann, J. Am. Chem. Soc., 100 (1978) 3686.
33 J. Hinze and H.H. Jaffé, J. Am. Chem. Soc., 67 (1963) 1501.
34 E. Canadell, O. Eisenstein and T. Hughbanks, Inorg. Chem., 23 (1984) 2435.
35 SHELXTL PLUS program package, Siemens Analytical X-ray Instruments Inc., Madison, WI.
36 International Tables for X-Ray Crystallography, Vol. IV, Kynoch, Birmingham, England, 1974.
37 Tables of the anisotropic temperature factors, a complete list of distances and angles, atomic parameters of the H atoms, as well as observed and calculated structure factors have been deposited at the Fachinformationszentrum Karlsruhe, Gesellschaft für wissenschaftlich-technische Information mbH, D-76344 Eggenstein-Leopoldshafen, Germany, and can be obtained by quoting the journal, authors and the file number CSD-57410.